## 8.1 Introduction

In the past few years, the fabrication of 'artificial enzymes,' i.e., mimetic nanoscale materials has oozed out as an excellent probe for the colorimetric detection which has attracted the researchers engaged in the biomaterials and biosensing (Chen *et al*. 2016, Lin *et al*. 2015). These artificial enzymes are more advantageous than natural enzymes because these enzymes possess excellent stability over a wide range of pH and temperature, and higher sensitivity (Lin *et al*. 2015, Xie *et al*. 2012). In addition to this, the artificial enzymes are economical with a tuned catalytic activity which makes it a promising probe for the colorimetric detection. Since, the first report on the preparation of artificial enzyme (Gao *et al*. 2007), several nanoscale materials have been successfully fabricated as an artificial enzymes such as $Co_3O_4$ (Yin *et al*. 2012), $CeO_2$ (Su *et al*. 2012), $V_2O_5$ (André *et al*. 2011), PdNPs (Shi *et al*. 2015a), PtNPs (Lin *et al*. 2015), AuNPs (Jv *et al*. 2010, Yan *et al*. 2017), CNTs (Song *et al*. 2010, Cui *et al*. 2011, Shin *et al*. 2017), GO (Zhang *et al*. 2017a), and CQDs (Long *et al*. 2016). Among these nanomaterials, AuNPs have attracted the researchers most because of its extraordinary biocompatible, easy preparation, catalytic, optical and electronic properties at the nanoscale (Shi *et al*. 2012). But expensiveness and aggregation at lower pH limit the catalytic performance of AuNPs. Therefore, with the objective aimed at reducing the cost of AuNPs catalysis, improving the dispersion and stability, AuNPs are needed to be loaded on a suitable support.

Currently, graphene-based nanomaterials have been extensively used as a supporting material because of its several unique properties such as lower cost, large surface area, electrical and thermal conductivity and excellent reliability (Chen *et al*. 2014). The previous studies revealed that only a few authors had demonstrated the successful dispersion of

AuNPs over the graphene sheets. However, to the best of our knowledge, only a few authors have reported the AuNPs@graphene nanocomposite as an 'artificial enzyme' (Liu *et al*. 2012a, b). Till date, there are no reports on the utilization of negatively charged AuNPs as an artificial enzymes synthesized from leaf extracts. The major advantages of using leaf extract synthesized AuNPs includes the high stability, biocompatibility, and low-cost synthesis with excellent catalytic activity. The large surface area of the graphene and above-mentioned properties of AuNPs synthesized from leaf extract encouraged us to fabricate the AuNPs@graphene nanocomposite to investigate the artificial enzyme-like activity, i.e., peroxidase-like activity.

Cholesterol is a steroid molecule which plays an important role in the life of cells (Li *et al*. 2011). It is required to maintain the structural integrity and fluidity of the membrane over the range of physiological temperatures (Nirala *et al*. 2015a). Apart from the major structural constituent of plasma membranes, it also plays an important role in the synthesis of steroid hormones, bile acid, and vitamin D (Cao *et al*. 2013, Qian *et al*. 2015). Due to all these essentialities, the cholesterol is synthesized by the cell from simple precursor molecules. The normal free cholesterol concentration in human serum is range from 1.0 - 2.2 mM (Zhao *et al*. 2008). Although cholesterol is very important for the organism, its uncontrolled production by the cell can lead to several diseases such as arteriosclerosis, hypertension, malabsorption, brain thrombosis, and myocardial infarction (Wu *et al*. 2017, Lin *et al*. 2017). As a clinical diagnosis, food safety, and environmental monitoring purpose, the quantitative estimation of cholesterol is very important (Li *et al*. 2011). Therefore, it is very important to develop analytical methods for highly selective and sensitive detection of cholesterol concentration. So far, various methods have been developed for the quantitative

determination of the cholesterol level in human blood serum such as fluorescence-based assay (Sun *et al*. 2017), liquid chromatography (Grün and Besseau 2016), molecular imprinting polymer (MIP) technology (Liu *et al*. 2017), electrochemical methods (Nantaphol *et al*. 2015, Cai *et al*. 2013), colorimetric enzymatic assay (He *et al*. 2017, Nirala *et al*. 2015b), and gas chromatography (Wu *et al*. 2009). Although the above-mentioned methods are very sensitive with lower detection limit, the need of technical skills, expensive equipment, and time-consuming procedures of sample preparation limits the applicability of these methods (Yang *et al*. 2016, Zhang *et al*. 2017b). Therefore, the fabrication of inexpensive and simple sensors has become an urgent need for the rapid and sensitive detection of cholesterol.

In the present investigation, we have fabricated the AuNPs@graphene nanosensor for the colorimetric detection of cholesterol. To be best of our knowledge, the negatively charged AuNPs synthesized from plant extracts have not been utilized to prepare an artificial enzyme for the colorimetric detection of cholesterol.

## 8.2 Materials and methods

### 8.2.1 Fabrication of AuNPs@rGO nanocomposite

The fabrication of AuNPs@rGO nanocomposite is given in chapter 2 under section 2.3.

### 8.2.2 Experimental methodology

The UV–Visible spectrophotometer (Evolution 201, Thermo Scientific) was used for the preliminary study of AgNPs in the range of 300 to 800 nm. The involvement of various functional groups was investigated using Fourier transform infrared spectrophotometer (FTIR, Perkin Elmer Spectrum 100) in the range of 4000–400 $cm^{-1}$. The X-ray

Diffractometer (Rigaku Miniflex II) having Cu Kα radiation source and Ni filter was applied to investigate the crystallinity of the synthesized AgNPs in the range of 20° to 80° and at a scanning rate of 6° $min^{-1}$ with 0.02° of step size. Primarily, the size and shape of the AgNPs was investigated using Field Emission Scanning Electron Microscopy with Energy-dispersive X-ray (FE-SEM-EDX, Hitachi H-7100). The elemental speciation and the purity were confirmed by EDX analysis. The Transmission Electron Microscopy (TEM, TECNAI 20 G2) at accelerating voltage 200 kV was used to confirm the shape and size of the biosynthesized AgNPs. The Selected Area Electron Diffraction (SAED) demonstrated the concentric diffraction rings which also confirmed the crystallinity of the synthesized AgNPs. The X-Ray Photoelectron Spectroscopy (XPS, AMICUS, Kratos Analytical, A Shimadzu) with Mg Ka (1253.6 eV) radiation as an X-ray source was conducted for the speciation of the nanocomposite. The fabricated AuNPs@RGO showed peroxidase-like mimetic activity which was applied for the colorimetric detection of cholesterol. The detailed experimentation is given in chapter 2 under section 2.5

## 8.3 Results and discussion

### 8.3.1 Characterization

Primarily, the formation of AuNPs, GO, rGO, and AuNPs@rGO was confirmed by UV- visible spectroscopy which are shown in **Figure 8.1**. The UV-visible spectra of AuNPs showed a sharp peak at 534 nm corresponding to its characteristic surface plasmon resonance (SPR) with $\lambda_{max}$ in the range of 500-600 nm. UV-visible spectra of GO represented the characteristic peaks at 230 nm and 300 nm which corresponded to the $\pi$–$\pi^*$ transition of C=C and n-$\pi^*$ transition of C=O respectively (Khanra *et al*. 2012). **Figure 8.1** revealed the absorption spectra of rGO with a red shift from 230 nm to 270 nm which corresponded to the

$\pi-\pi^*$ transition of a C=C bond. This shifting clearly indicated the successful reduction of GO into rGO with the restoration of a C=C bond (Gupta and Saha 2012). **Figure 8.1** also revealed the UV-visible spectra of AuNPs@rGO nanocomposite which depicted both the peak of AuNPs and rGO with minute shifting. The shifting in these peaks might be due to the interaction of AuNPs with the surface of rGO to form AuNPs@rGO nanocomposite.

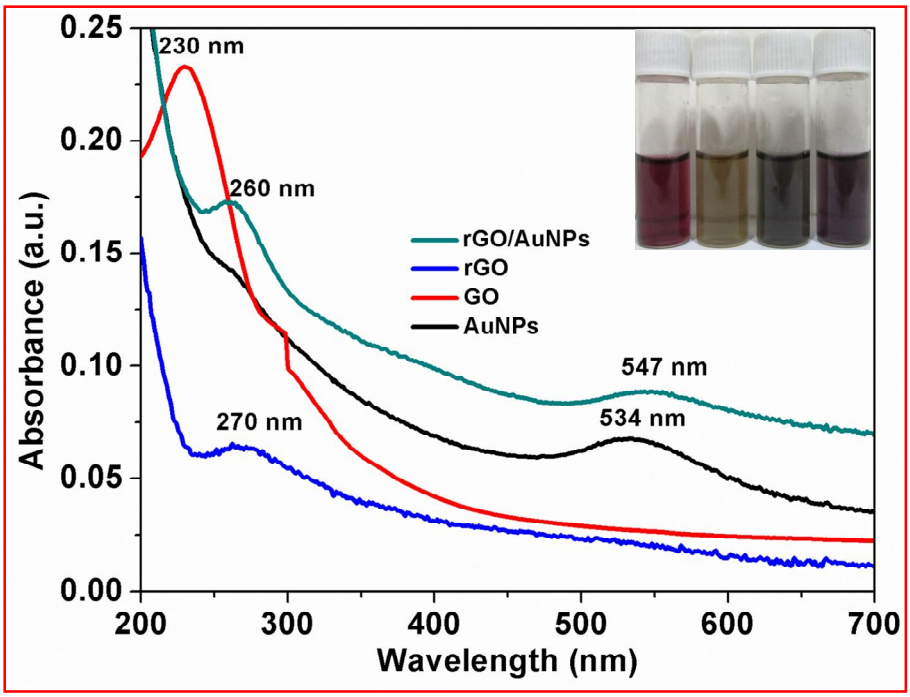


**Figure 8.1 UV-visible spectra of AuNPs, GO, rGO, AuNPs@rGO**

Thus prepared AuNPs@rGO nanocomposite was further characterized through FTIR analysis to investigate the various functional groups of AuNPs, GO, rGO and their involvement in the formation of AuNPs@rGO nanocomposite **Figure 8.2**. The figure showed that the FTIR spectrum of green synthesized AuNPs revealed the absorption band at 3421 $cm^{-1}$, 2922 $cm^{-1}$, 2852 $cm^{-1}$, 1632 $cm^{-1}$, and 1061 $cm^{-1}$. The band at 3421 $cm^{-1}$, 2922 $cm^{-1}$,

2852 $cm^{-1}$, corresponded to the presence of stretching vibration ($\upsilon_s$) of OH, C=C-H, and C-H respectively. Whereas the band at 1632 $cm^{-1}$, and 1061 $cm^{-1}$, were due to the presence of $\upsilon_s$ of C=C, and O-C respectively (Kumar *et al*. 2017). The FTIR spectrum of GO corroborated the characteristic bands at 3409 $cm^{-1}$, 2927 $cm^{-1}$, 2852 $cm^{-1}$, 1735 $cm^{-1}$, 1665 $cm^{-1}$, 1374 $cm^{-1}$, and 1050 $cm^{-1}$ which were due to the $\upsilon_s$ of OH, $\upsilon_s$ of $sp^2$ hybridized C-H, $\upsilon_s$ of $sp^3$ hybridized C-H, $\upsilon_s$ of C=O carbonyl, $\upsilon_s$ of C=C, $\upsilon_b$ of C-OH, and $\upsilon$s of epoxide (Gao *et al.* 2011).

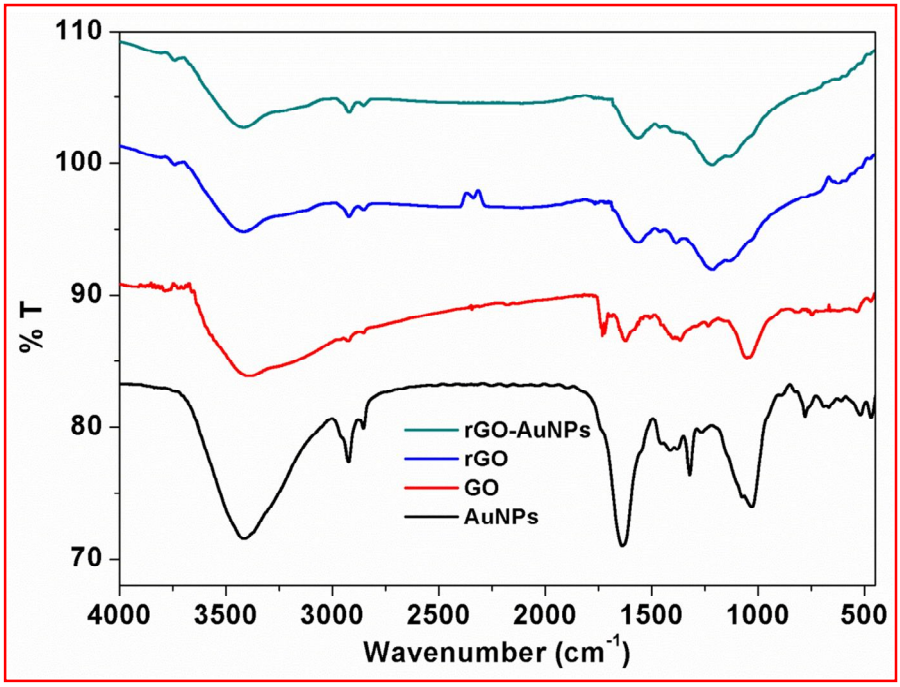


**Figure 8.2 FTIR spectra of AuNPs, GO, RGO, AuNPs@rGO**

The FTIR spectrum of rGO exhibited that the peak present at 1735 $cm^{-1}$ (C=O carbonyl) shifted to a 1565 $cm^{-1}$ ($sp^2$ hybridized C=C) and the peak present at 1050 $cm^{-1}$ disappeared. The disappearance of peak at 1050 $cm^{-1}$ ($\upsilon_s$ of epoxide), as well as shifting of 1735 $cm^{-1}$ peak to 1565 $cm^{-1}$ advocated the conversion of GO to rGO by removal of surface oxygenated groups which was in accordance with the results obtained from UV-visible

spectra (Gao *et al*. 2011). The reduction of GO into rGO is also advocated by the change in color of the solution from brown to dark black (**Inset Figure 8.1**).

The crystalline nature of the synthesized AuNPs, GO, rGO, and AuNPs@rGO nanocomposite was investigated through XRD analysis (**Figure 8.3)**. The XRD analysis was carried out at the scanning rate of 6° $min^{-1}$ and step size of 0.02° in the angular range $20° \leq 2\theta \leq 80°$. From the results, it is confirmed that the XRD spectrum of AuNPs showed the diffraction peaks at $2\theta = 38.06°$, 44.24°, 64.47°, and 77.3°. These peaks were well matched with the JCPDS file no. 040784 and corresponding to (111), (200), (220) and (311) Bragg's reflections which advocated the crystalline planes of metallic gold with face-centered cubic (fcc) crystals. The XRD spectrum of GO showed the presence of characteristics diffraction peak of GO at $2\theta = 10.9°$ corresponding to the 002 Bragg's reflections. The significantly expanded *d*-spacing of GO (0.83 nm) comparatively pristine graphite (0.34 nm) confirmed its successful exfoliation. This exfoliation suggested the inclusions of oxygen-containing functional groups and water molecules between the graphitic layers. When the GO was reduced, the diffraction peak present at $2\theta = 10.9°$ got disappeared and showed the appearance of the broad diffraction peak at $2\theta = 23.9°$ and 43.0°. These peaks corresponded to (002) and (011) Bragg's reflections respectively having 0.418 nm of *d*-spacing. The decreased *d*-spacing of rGO advocated the removal of intercalated oxygen-containing functional groups and the broad peaks suggested the amorphous nature of rGO along stacking direction of its sheet. The XRD spectra of AuNPs@rGO revealed the presence of a characteristic peak of rGO and AuNPs confirming the AgNPs-rGO nanocomposite formation.

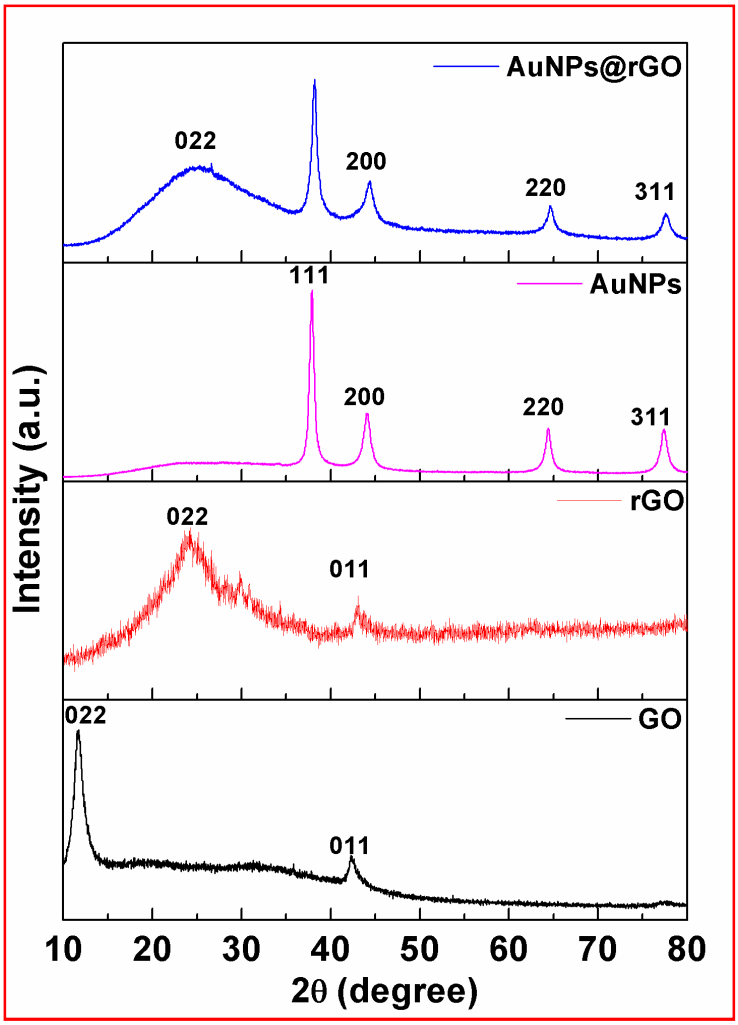


**Figure 8.3 XRD patterns of GO, rGO, AuNPs, and AuNPs@rGO**

The exact size and shape of the AuNPs were studied through TEM analysis. The TEM images of the optimum AuNPs (1.6 mM $HAuCl_4.xH_2O$) synthesized from an aqueous extract of *Croton bonplandianum* (AEC) is shown in **Figure 8.4A**. The TEM images corroborated the presence of spherical AuNPs in the range from 1 to 19 nm. The size distribution histogram of AuNPs corresponding to TEM image revealed that the average size of AuNPs was of 8.6 nm where maximum AuNPs were in the range of 5 nm to 7 nm (**Inset Fig. 8.4A)**. The TEM image of bare rGO sheet is shown in **Figure 8.4B** which is devoid of

any AuNPs. The fabricated AuNPs@rGO is shown in Figure 8.4 C and D at different magnifications clearly which corroborated the distribution AuNPs at the rGO sheets showed the clear sheet of rGO which indicated the successful formation of AuNPs@rGO.

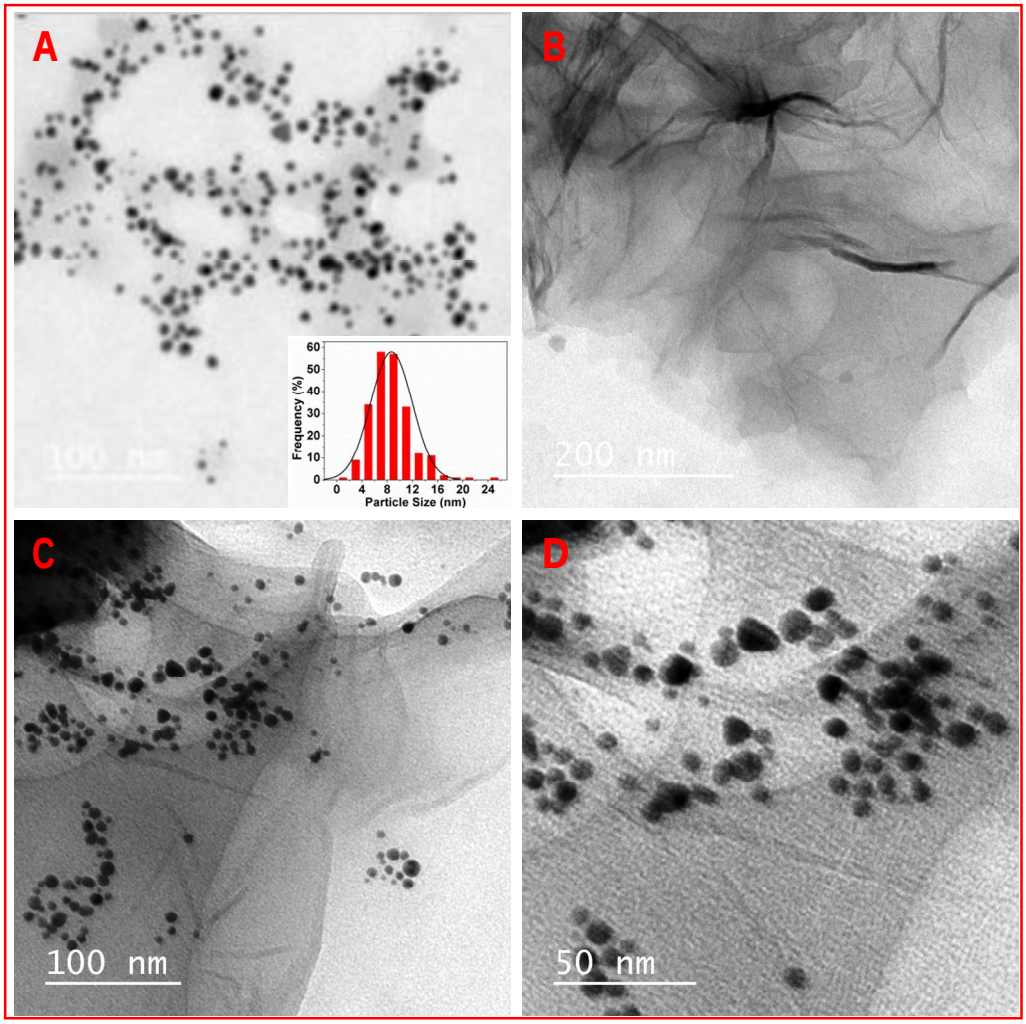


**Figure 8.4 TEM images of AuNPs (A), bare rGO sheet (B), AuNPs@rGO at different magnifications (C and D)**

### 8.3.2 Peroxidase-like activity

The peroxidase-like activity of each AuNPs, rGO, and AuNPs@rGO was investigated on the basis of development of blue color due to the oxidation of chromogenic TMB after interacting with $H_2O_2$. When the AuNPs@rGO was added into the TMB+$H_2O_2$ system, $H_2O_2$ get decomposed into $OH^{\bullet}$ radical which is accelerated by the redox reaction occurring at the surface of AuNPs@rGO.

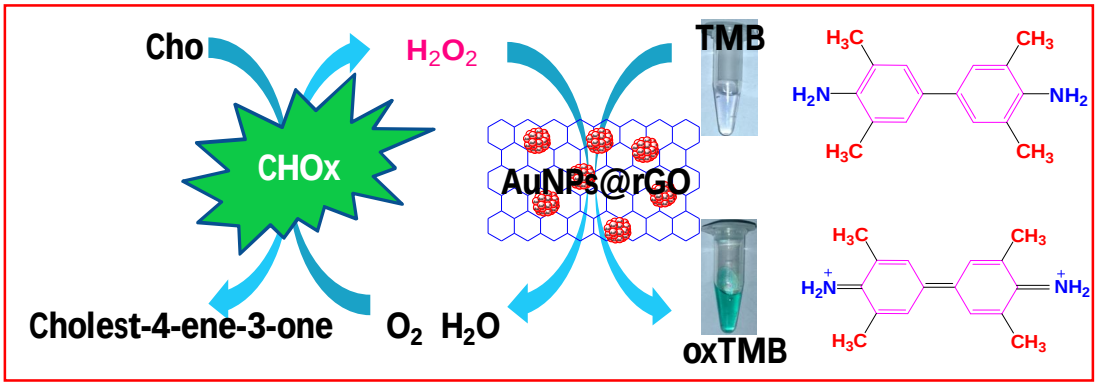


**Scheme 8.1 Schematic illustration of peroxidase-like activity of AuNPs@rGO and colorimetric detection of cholesterol using cholesterol oxidase and AuNPs@rGO**

The $OH^{\bullet}$ radical thus generated abstract the electron from the reduced TMB and turned it into the dark blue colored oxTMB having characteristics absorbance at 652 nm. The catalytic action of the ChOx on ChO releases $H_2O_2$ and cholest-4ene-3-one as a by-product in the presence of oxygen (Nirala *et al*. 2015b, Shi *et al*. 2015b). The $H_2O_2$ produced in this reaction can be quantitatively used for the oxidation of TMB into oxTMB in the presence of AuNPs@rGO (**Scheme 8.1**). The above fact encouraged us for the colorimetric detection of cholesterol.

The peroxidase-like activity of each AuNPs, rGO, and AuNPs@rGO was investigated by monitoring the UV-visible spectra of the oxidized blue color product of TMB (OxTMB) which gives sharp spectra at 652 nm. From the figure, it is obvious that the absence of

characteristic peak of the OxTMB at 652 nm indicated that the rGO was not independently able to mimic peroxidase activity (**Figure 8.5**). This was due to the fact that the fused layers of rGO create difficulty in adsorption of substrates on to its surface along with a forbidden transfer of electron. Although the AuNPs showed the presence of spectra at 652 nm but it was not intense as of AuNPs@rGO which revealed the better catalytic activity of AuNPs@rGO

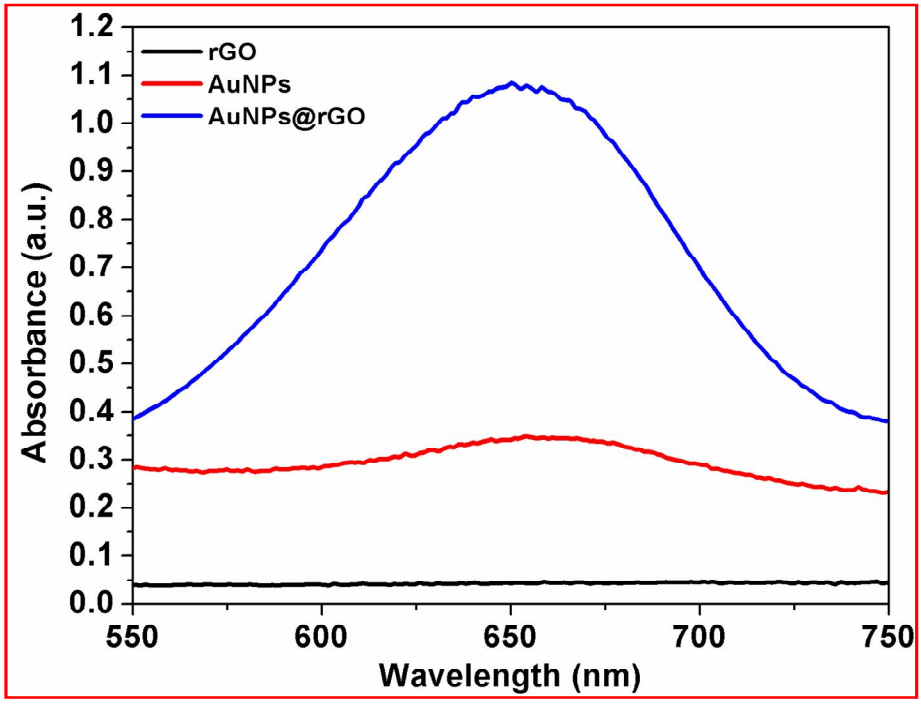


**Figure 8.5 Showing the change in absorbance at 652 nm for rGO, AuNPs and AuNPs@rGO (50 µL) with TMB (50 µL, 1 mM) and $H_2O_2$ (50 µL, 1 mM) in 200 µL of 0.2 M NaAc buffer solution (pH 4.0) at 37 °C after 10 min of incubation period**

With the aim of investigating the role of each constituent of different composition ($H_2O_2$, TMB, TMB+$H_2O_2$, AuNPs@rGO+TMB, and AuNPs@rGO+TMB+ $H_2O_2$) in the development of deep blue color and the intense absorption of the OxTMB at 652 nm, the time-dependent absorbance changes at 652 nm was monitored (**Figure 8.6**). It was observed

that the absorbance spectra for $H_2O_2$, TMB alone and AuNPs@rGO+TMB without $H_2O_2$ did not reveal the change in absorbance with time. The absorbance spectra of TMB+$H_2O_2$ showed a negligible change in absorbance at 652 nm due to the low reaction rate of TMB and $H_2O_2$. When AuNPs@rGO was added into the TMB+$H_2O_2$ system, a deep blue color (**Inset Figure 8.6**) and considerable change in absorbance at 652 nm was observed within 5 min which confirmed its peroxidase-like activity.

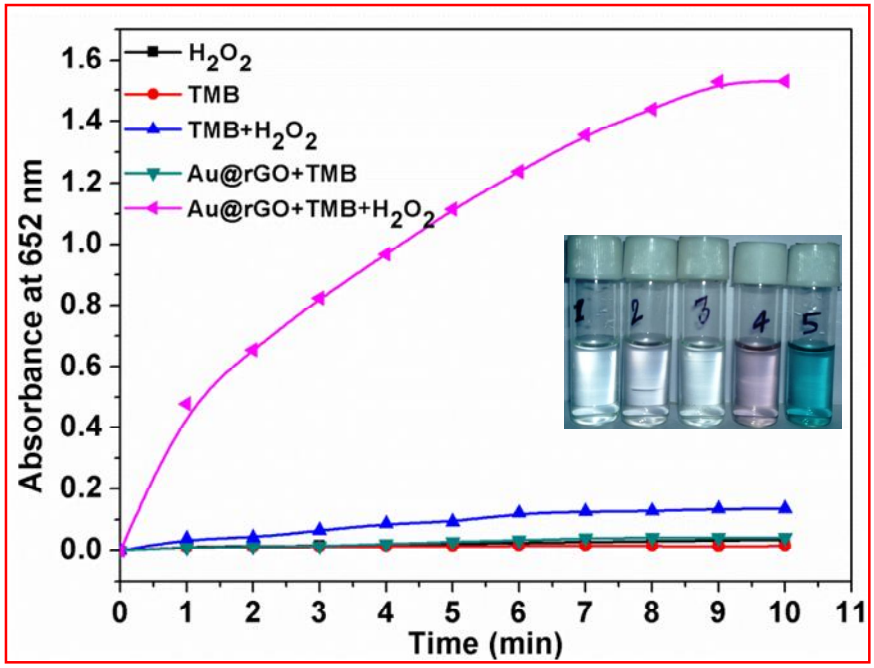


**Figure 8.6 Changes in absorbance of different constituents with time at 652 nm (1) $H_2O_2$ (50 µL, 1 mM), (2) TMB (50 µL, 1 mM), (3) TMB (50 µL, 1 mM) + $H_2O_2$ (50 µL, 1 mM), (4) Au@rGO ((50 µL) + TMB (50 µL, 1 mM), (5) Au@rGO (50 µL) + TMB (50 µL, 1 mM) + $H_2O_2$ (50 µL, 1 mM) in 200 µL of 0.2 M NaAc buffer solutions (pH 4.0). Inset figure showed the photograph of the respective reaction system**

### 8.3.2.1 Optimization of the factors affecting peroxidase-like activity

It is well known that the catalytic activity of the natural enzymes is greatly affected by lower and higher value of pH and temperature. In addition to this, the catalytic activity of the natural enzymes is also affected by the change in concentrations of the reaction system constituents. Therefore, the various factors affecting the peroxidase-like catalytic activity of AuNPs@rGO such as incubation time, pH, temp, TMB concentration, $H_2O_2$ concentration, and AuNPs amount were optimized using one parameter at a time approach for obtaining the optimum result for the better performance of the detection of cholesterol.

**Figure 8.7A** showed the effect of pH on the peroxidase-like activity of AuNPs@rGO in 0.2 M NaAc buffer at different pH in the range of 1-10. The figure clearly corroborated that the peroxidase-like activity of AuNPs@rGO was excellent in acidic condition and the optimum pH 4.

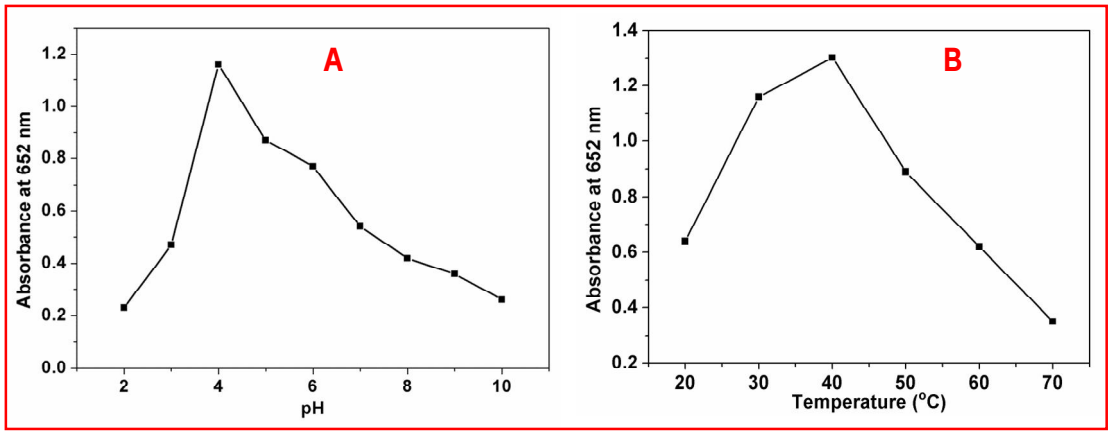


**Figure 8.7 Peroxidase-like activity of AuNPs at different (A) pHs (2 – 10) at 37 $^{o}$C, and (B) temperatures, (20 – 70 $^{o}$C) at pH 4 using AuNPs@rGO (50 µL) + TMB (50 µL, 1 mM) + $H_2O_2$ (50 µL, 1 mM) in 200 µL of 0.2 M NaAc buffer solution**

This peroxidase-like activity started to decrease with the further increase in pH and negligible at higher pH. Since it is reported that at higher pH, $H_2O_2$ get decomposed into $H_2O$

and $O_2$ rather $OH^{\bullet}$ radical (Feng *et al*. 2017). Similarly, the effect of temperature on the peroxidase-like activity of AuNPs@rGO was studied and observed that the peroxidase-like activity was optimum at temp 40 ºC. Further, on increasing the temperature, the peroxidase-like activity decreased due to agglomeration of AuNPs@rGO which hindered the transfer of electron (Feng *et al*. 2017) (**Figure 8.7B)**. Similarly, the effect of different constituents of the AuNPs@rGO reaction system like the amount of AuNPs@rGO and concentrations of TMB and $H_2O_2$ were also optimized at constant incubation time (9 min), pH 4, and temp 40 ºC.

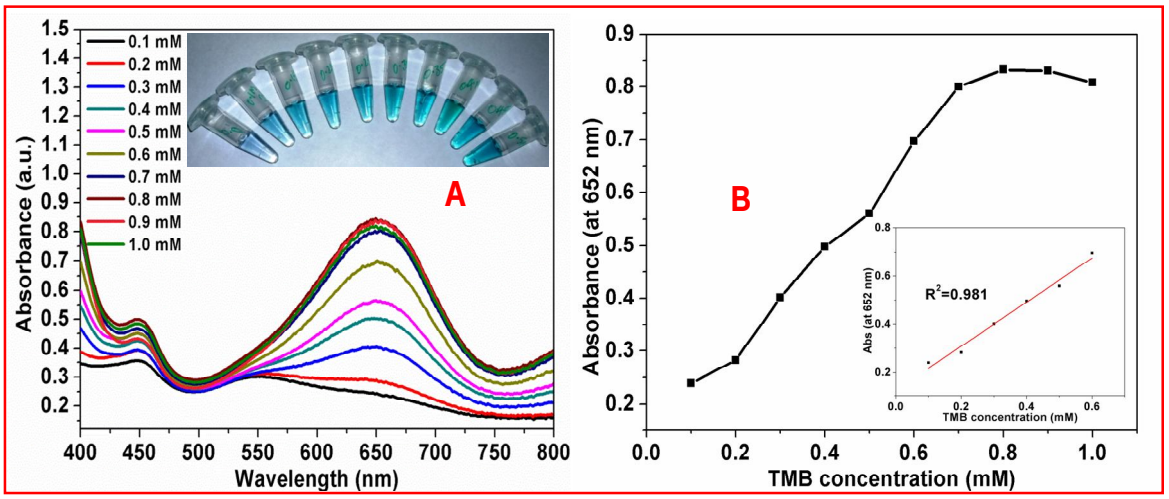


**Figure 8.8 Peroxidase-like activity of AuNPs@rGO at pH 4 and temp 40 ºC at (A) different concentrations of TMB (0.1 mM to 1 mM) using 50 µL of 1 mM $H_2O_2$ and 50 µL AuNPs@rGO in 200 µL of 0.2 M NaAc buffer at 9 min of fixed incubation time with inset photographs of corresponding change in color, (B) relationship between absorbance and TMB concentrations with inset calibration plot showing the linear relationship between 0.1 to 0.6 mM with $R^2$ = 0.981**

It was observed that the concentration of TMB and $H_2O_2$ and the amount of AuNPs@rGO being too high or too low was not suitable for the better peroxidase-like activity of AuNPs@rGO. While optimizing the TMB concentration, it was observed that 0.8 mM was the optimum TMB concentration using 50 µL $H_2O_2$ (1 mM) and 50 µL

AuNPs@rGO in 200 µL NaAc buffer for the better peroxidase-like activity of AuNPs@rGO (**Figure 8.8A)**.

**Inset Figure 8.8B** represented the linear relationship between 0.1 mM to 0.6 mM with $R^2$ = 0.981. **Figure 8.9A** and **B** showed that 80 µL of AuNPs@rGO amount was the optimum amount for better peroxidase-like activity at 50 µL $H_2O_2$ (1 mM) and 50 µL TMB (0.8 mM) which revealed the linear relationship between 10 µL to 60 µL AuNPs@rGO with $R^2$ = 0.997.

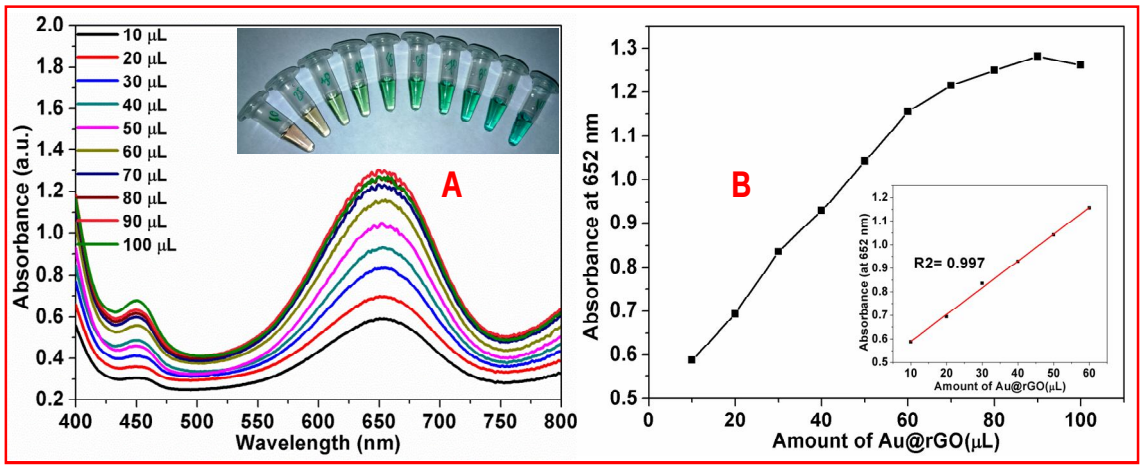


**Figure 8.9 Peroxidase-like activity of AuNPs@rGO at (A) different amount of AuNPs@rGO using 50 µL of 0.1 mM $H_2O_2$ and 50 µL of 0.8 mM TMB in 200 µL NaAc buffer of 0.2 M at constant pH 4 and temp 40 $^oC$ and incubation time 9 min with inset photographs of corresponding change in color, (B) relationship between absorbance and AuNPs@rGO amount with inset calibration plot showing the linear relationship between 10-60 µL with $R^2$ = 0.997**

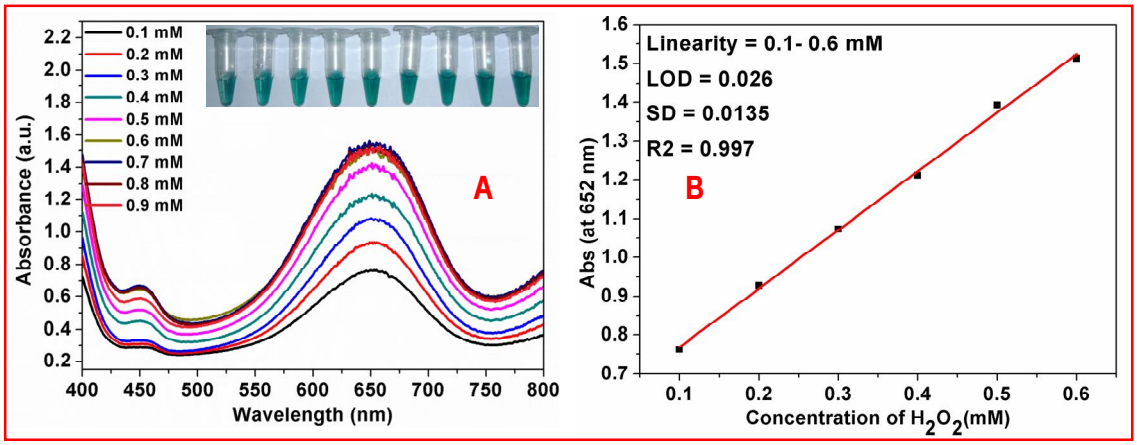


**Figure 8.10 (A) Peroxidase-like activity of AuNPs@rGO at (A) different concentrations of $H_2O_2$ using 80 µL AuNPs@rGO and 50 µL of 0.8 mM TMB in 200 µL NaAc buffer of 0.2 M at constant pH 4 and temp 40 $^oC$ and fixed incubation time 9 min with inset photographs of corresponding change in color, (B) relationship between absorbance and concentrations of $H_2O_2$ with inset calibration plot showing the linear relationship between 0.1 to 0.6 mM with $R^2$ = 0.997**

**Figure 8.10A** and **B** indicated that 0.8 mM $H_2O_2$ concentration was the optimum concentration observed at 80 µL AuNPs@rGO and 50 µL of 0.8 mM TMB. **The Inset Figure 8.10B** represented the linear calibration plot of $H_2O_2$ which showed the linear relationship between 0.1 mM to 0.6 mM with $R^2$ = 0.997. The linear regression equation was $A_{652\ nm}$ = 1.510C+0.618 where the limit of detection for $H_2O_2$ was found to be 0.0268 mM.

This $H_2O_2$ can be produced through the catalytic oxidation of cholesterol (ChO) by cholesterol oxidase (ChOx) which encouraged us to develop the facile colorimetric detection technique of cholesterol.

### 8.3.2.2 Detection of cholesterol

After the detection of $H_2O_2$, the efficacy of the fabricated AuNPs@rGO was applied for the selective and sensitive detection of cholesterol by quantifying the released $H_2O_2$ through the catalytic action of ChOx on ChO. For the detection purpose, different concentrations of ChO in 0.1 mM PBS (pH 7.0) were treated with 20 µL of ChOx (1 mg/mL)

and incubated for 10 min at 37 ºC and incubated for 10 min in dark. Thereafter, the optimum component of the reaction system i.e. 80 µL AuNPs@rGO, 50 µL of 0.8 mM TMB were added in 200 µL NaAc buffer solutions of 0.2 M having pH 4.0. Thereafter, the corresponding UV-visible spectra were recorded with maximum absorbance at 652 nm.

By using the maximum absorbance data at 652 nm, the calibration curve of the ChO was plotted which showed the linear relationship between 0.2 to 1.2 mM with $R^2$ = 0.996. The linear regression equation was $A_{652\ nm}$ = 0.547C+0.170 and the LOD was calculated to be 0.062 mM using the formula: LOD = 3(SD/B) where SD is the standard deviation and B is the slope of the calibration curve (**Figure 8.11A and B)**. The LOD obtained in our experiment was satisfactory as compared to previously reported papers which are given in **Table 8.1.**

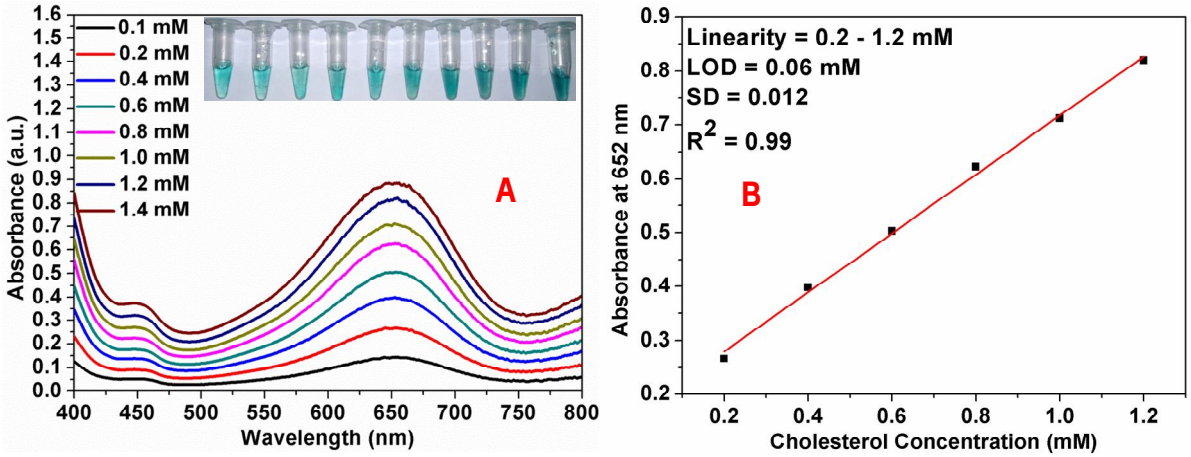


**Figure 8.11 (A) UV-visible spectra of different concentrations of ChO in the presence of AuNPs@rGO + TMB + ChOx (B), the calibration curve of cholesterol showing the linear relationship between 0.2 to 1.2 mM with $R^2$ = 0.99**

**Table 8.1 Comparison table showing the different materials used for the detection of ChO**

| **Sensing element** | **Sensing method** | **Linear range** | **Detection limit** | **Reference** |
|---|---|---|---|---|
| GQDs | Colorimetric | 0.02-0.6 mM | 0.006 mM | Nirala *et al*. 2015a |
| ChOx/DNAzymes | Colorimetric | 1-30 mM | 0.1 M | Li *et al*. 2012 |
| ChOx/peroxidase | Colorimetric | 0-7 mM | - | Viturro *et al*. 2009 |
| $MoS_2$ NR–Au NP | Colorimetric | 0.04-1.0 mM | 0.015 mM | Nirala *et a*l. 2015b |
| Pt/PCN | Colorimetric | - | $8.3 \times 10^{-6}$ M | Shi *et al*. 2015a |
| (MWNTs) – Au/PPD–ChOx | Amperometric | $5.0\times10^{-4}$ – $6.0\times 10^{-3}$ M | $2.0\times10^{-4}$ M | Guo *et al*. 2004 |
| ChOx/haemoglobin | Amperometric | 10-600 M | 9.5 M | Zhao *et al*. 2008 |
| AuNPs@rGO | Colorimetric | 0.2 to 1.2 mM | 0.062 mM | Present work |

### 8.3.2.3 Selectivity

To investigate the selectivity of the fabricated AuNPs@RGO, the experiment was performed by adding 50 µL of 1 mM of different possible analytes present in blood serum (for example, ascorbic acid, uric acid, xanthine, urea, beta-sterol, stigmasterol and cholesterol) into the same reaction system used for ChO detection (**Figure 8.12**). It was observed that ChO showed the highest selectivity having maximum absorbance intensity amongst all the analytes. Thus, the fabricated system can be applied for the selective colorimetric detection of ChO. **Figure 8.13A** indicated the consistency of results obtained from the fabricated AuNPs@rGO when the experiment was performed 6 times in the same set of experimental conditions. The consistency in results of reproducibility obtained using five samples at the same set of experimental conditions is also shown in **Figure 8.13B**.

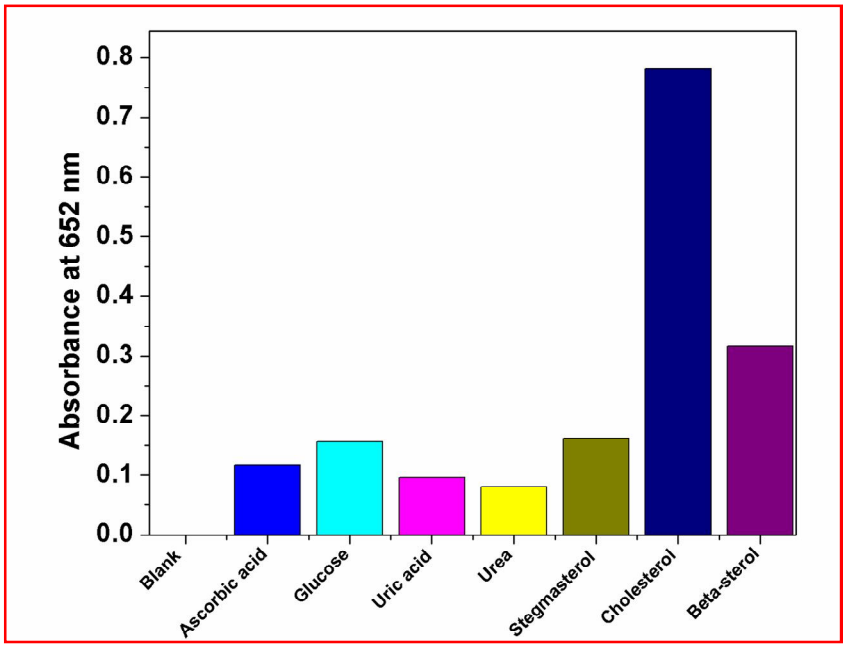


**Figure 8.12 Selectivity of AuNPs@rGO towards ChO among different analytes present in serum using 50 µL TMB of 0.8 mM, 80 µL AuNPs@rGO, 200 µL NaAc buffer of 0.2 M (pH 4), and 20 µL ChOx of 1 mg/mL**

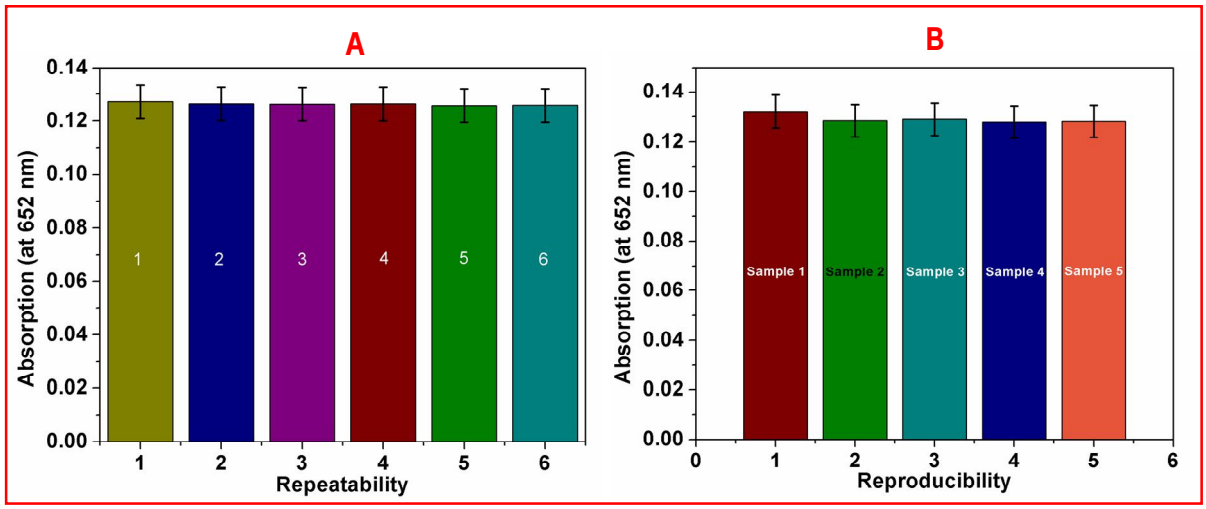


**Figure 8.13 Repeated experiments for 6 times using 50 µL TMB of 0.8 mM, 80 µL AuNPs@rGO in 200 µL NaAc buffer of 0.2 M (pH 4), 100 µL ChO in PBS (0.1 mM, pH 7.0), and 20 µL ChOx of 1 mg/mL (A), reproducibility of samples using same experimental condition**

## 8.4 Conclusion

The present work deals with the peroxidase like-mimetic activity of AuNPs@rGO. The AuNPs@rGO was fabricated using plant extracts synthesized AuNPs and rGO obtained by the reduction of GO prepared by modified hummer's method. The utilization of negatively charge plant extract synthesized AuNPs has not been reported yet for the fabrication of AuNPs@rGO for peroxidase-like mimetic activity. Several characterizing techniques such as UV-visible spectroscopy, FTIR, XRD, and TEM advocated the successful fabrication of AuNPs@rGO. The TEM images revealed the clear sheets of rGO and uniformly distributed AuNPs over its surface. Thus prepared AuNPs@rGO showed an excellent peroxidase-like activity which influenced by the change in pH, and temperature. The other variables affecting the catalytic activity of the AuNPs@rGO like the concentration of TMB, and AuNPs@rGO amount were also optimized for securing optimum peroxidase-like activity of AuNPs@rGO. The fabricated AuNPs@rGO showed its catalytic activity as that of natural peroxidase enzyme because of its efficiency at lower pH and 40 ºC temperatures which were used in the colorimetric detection of $H_2O_2$ and cholesterol in human blood serum. In the current investigation, the typical limit of detection for $H_2O_2$ and ChO were 0.0268 and 0.062 mM respectively. Overall, a simple, cost-effective, rapid, highly sensitive and selective colorimetric method was proposed for the potential detection of cholesterol which would be helpful for the medical diagnosis and biochemistry based applications.

.